Published in final edited form as:
Neuropharmacology. 2009 January ; 56(1): 247–253. doi:10.1016/j.neuropharm.2008.08.021.

Demonstration of Functional α4-Containing Nicotinic Receptors in the Medial Habenula

Carlos Fonck[1,§], **Raad Nashmi**[2], **Ramiro Salas**[3], **Chunyi Zhou**[1], **Qi Huang**[1], **Mariella De Biasi**[3], **Robin A. J. Lester**[4], and **Henry A. Lester**[1]

1*Division of Biology, California Institute of Technology, Pasadena, CA 91125*

2*Department of Biology, University of Victoria, BC, Canada, V8W 3N5*

3*Department of Neuroscience, Baylor College of Medicine, Houston, TX 77030*

4*Department of Neurobiology & Evelyn F. McKnight Brain Institute, University of Alabama at Birmingham, Birmingham, AL, 35294*

Abstract

The medial habenula (MHb) exhibits exceptionally high levels of nicotinic acetylcholine receptors (nAChRs), but it remains unclear whether all expressed nAChR subunit mRNAs are translated to form functional receptors. In particular α4 subunits have not been reported to have any functional role, despite strong α4 mRNA expression in the ventrolateral MHb. We studied a strain of knock-in mice expressing fluorescent α4* nAChRs (α4YFP), as well as a knock-in strain expressing hypersensitive α4* nAChRs (α4L9′A). In α4YFP mice, there was strong fluorescence in the ventrolateral MHb. In hypersensitive α4L9′A mice, injections of a low dose of nicotine (0.1 mg/kg) led to strong c-fos expression in only the ventrolateral region of the MHb, but not in the MHb of wild-type (WT) mice. In MHb slice recordings, ventrolateral neurons from α4L9′A mice, but not from WT mice, responded robustly to nicotine (1 μM). Neurons in the medial aspect of the MHb had >10-fold smaller responses. Thus α4*-nAChRs contribute to the selective activation of a subset of MHb neurons. Subunit composition analysis based on gain-of-function knock-in mice provides a useful experimental paradigm.

Keywords

addiction; ion channel; c-fos; knock-in; mRNA

Introduction

Nicotinic acetylcholine receptors (nAChRs) are promising drug targets in the treatment of several CNS disorders such as Alzheimer's disease, schizophrenia, neuropathic pain and substance abuse (Arneric et al., 2007). Successful treatments will require discovery of agents that select among multiple subtypes of nAChRs (Role, 1992; Gotti et al., 2007). To choose appropriate drugs and to avoid off-target effects, one must understand how each nAChR is

Corresponding author: Robin A.J. Lester, Department of Neurobiology, SHEL 1006, University of Alabama at Birmingham, 1825 University Blvd, Birmingham, Al 35294-2182, Tel: (205) 934-4483, Fax: (205) 934-6571, Email: rlester@nrc.uab.edu.
§Present address: AstraZeneca Pharmaceuticals LP, Wilmington, DE 19850

distributed among cell types and contributes to neuronal function and behavior. Despite much progress (e.g. Luetje, 2004), these tasks remain challenging because we lack tools to unambiguously identify the subunit make-up of particular nAChRs. Novel subunit-specific toxins (Janes, 2005) and gene-specific knockout models (Cordero-Erausquin et al., 2000; Picciotto et al, 2001) have confirmed roles for certain subunits; however, the expression of multiple subunits within individual cells renders subunit compensation a possibility in knock-out studies (e.g., Brussaard, 1994).

Definitive identification of nAChR subtypes is especially problematic for neurons in the medial habenula (MHb), which expresses the highest levels of nAChRs in the brain (Marks et al., 1998). MHb expresses mRNAs encoding several different subunits (α3-α7 and β2-β4) (Sheffield et al., 2000). Pharmacological data suggest that heteromeric nAChRs, composed of a minimum of α3 and β4 subunits (α3β4*), are a major functional subtype in this nucleus (Mulle and Changeux, 1990; Quick et al., 1999; Perry et al., 2002; Whiteaker et al., 2002). While the function(s) of this small epithalamic nucleus is not well understood (Lecourtier and Kelly, 2007), α3β4*-nAChRs are important for sensitization and self-administration of opioids in rats (Glick et al., 2006; Taraschenko et al., 2007). It is not yet known how other nAChR subunits contribute to the heterogeneous MHb nAChR receptor population (Connolly et al., 1995). This paper examines the expression of functional α4 subunits, whose mRNA is also found within the MHb (Wada et al, 1989; Pauly et al., 1996). α4* nAChRs are thought to be necessary and sufficient for the expression of behaviors underlying nicotine addiction including reward, tolerance and sensitization (Tapper et al., 2004, Maskos et al., 2005), but not withdrawal (Salas et al, 2004). Also, α4β2* receptors are associated with monogenic epilepsies (Phillips et al., 1995, Fonck et al., 2003, 2005).

Here we combined conventional approaches with genetic strategies that use two lines of knock-in mice. One line expresses fluorescently-tagged α4* nAChRs (α4YFP, Nashmi et al., 2007); the other expresses hypersensitive α4* nAChRs bearing a leucine to alanine substitution at the M2 9′ position; (α4L9′A, Tapper et al., 2004; Fonck et al, 2005). The results show the distribution and function of MHb α4* nAChRs.

Materials and Methods

Experiments involving mice were performed following the guidelines established by each institution's Animal Care Committee. Mutant mouse lines were genotyped by PCR analysis of tail DNA.

In situ hybridization of the α4 subunit mRNA in MHb of C57BL/6J mice

A mouse DNA template encoding the third intracellular loop of the α4 nAChR subunit was prepared by RT-PCR amplification of mRNA from a mouse septal neuroblastoma cell line (SN56). The mouse DNA templates were subcloned into pBluescript SK(+) and sequenced. The genomic DNA region for α4 had a total of 743 bp (bases 1046–1789). cRNA riboprobes labeled with [^{35}S]UTP (Dupont NEN, Boston, MA) were synthesized from the mouse DNA templates. Post-fixed 20 μm sections from C57BL/6J mouse brains were processed for *in situ* hybridization. Slide-mounted sections were pre-incubated with 1 μg/ml proteinase K for 10 min at 22°C, then incubated for 18 h at 60 °C with a hybridization solution containing [^{35}S]UTP-labeled cRNA riboprobe (1×10^7 cpm/ml) in the antisense or sense orientation. The sense riboprobe gave no signal above background (not shown). Sections were Nissl stained (0.1% cresyl violet solution, Sigma-Aldrich, Saint-Louis, MO) to help visualize the MHb.

Generation and analysis of α4YFP mice

Generation and phenotypic characterization of α4YFP knock-in mice have been described (Nashmi et al 2007). Previous studies *in vitro* (Nashmi et al, 2003) and in the knock-in mice (Nashmi et al, 2007) showed that YFP inserted in the M3-M4 cytoplasmic loop did not alter the function or distribution of α4* receptors compared to WT. For fluorescence analysis, mice were sacrificed and fixed by intracardial perfusion with 4% paraformaldehyde in phosphate-buffered saline (PBS). Brain coronal sections, 30 μm thick, were sliced with a cryostat and mounted onto glass slides. Sections of the middle portion of the MHb along its rostro-caudual axis were selected for these studies. Fluorescence images were collected from a microscope equipped with a spectrally resolved detector array (LSM 510 Meta; Zeiss, Germany). Images (12-bit intensity resolution over 1024 × 1024 pixels) were collected at wavelengths between 495 and 602 nm with bandwidths of 10.7 nm during excitation of YFP with the 488 nm line of an argon laser (1-10%; 23 – 114 μW). Specific YFP fluorescence was isolated from background autofluorescence at each pixel with a linear unmixing algorithm based on two reference spectra: fluorescence of YFP and autofluorescence of WT brain sections.

C-fos immunoreactivity in nicotine-injected mice

Generation and phenotypic characterization of α4L9′A mice have been previously described (Tapper et al, 2004, Fonck et al, 2005, Shao et al, 2008). WT and homozygous α4L9′A mice were subcutaneously injected with 0.1 (n = 5 / genotype), 2 (n = 3 / genotype) or 10 (n = 3 WT) mg/kg nicotine 1.5 h prior to being euthanized with 2-bromo-2-cloro-1,1,1,-trifluoroethane. As a negative control, three WT and three α4L9′A mice were injected with saline 1.5 hr prior to euthanasia. Mice were perfused through the left ventricle with 0.1% heparin in PBS (10 ml) followed by 4% paraformaldehyde (20 ml). Brains were equilibrated in 25% sucrose before 30 μm thick coronal sections were cut with a cryostat. Brain sections from α4L9′A and WT mice were simultaneously processed. Free-floating sections were reacted against c-fos polyclonal antibody diluted 1:500 (Santa Cruz biotechnology, CA). The antigen-antibody signal was detected with a secondary antibody, amplified with an avidin-biotin reaction (Vector laboratories, Burlingame, CA) and visualized with diaminobenzidine (Sigma-Aldrich, Saint Louis, MO).

Initial observations indicated that the distribution pattern of c-fos positive cells was similar among sections from the rostral, middle and caudal regions of the MHb. Thus final quantification and statistical analysis were performed on matching (WT vs. α4L9′A) sections from the middle portion of the MHb, as for the fluorescence measurements on α4YFP mice. We compared two cell-counting methodologies: i) unbiased stereology using Stereo Investigator software (mbf-bioscience, Williston, VT) and ii) direct cell counting. The average number of c-fos positive cells counted within MHb sections was similar for the two methods. However, the standard deviation rendered by the unbiased stereology method was larger compared to direct counts. Unbiased stereology contributed more variability to our measurements because there was an uneven distribution of c-fos positive cells in the MHb. In other words, there were cell counts from quadrants in regions with many c-fos positive cells as well as counts from quadrants with very few or no positive cells. Consequently, we performed our analysis based on direct cell counts. Because the variance in the data was not randomly distributed in the saline-treated groups, a non-parametric test, Kruskal-Wallis, followed by Tukey's test for comparisons, was used to compare treatment groups (SigmaStat by Systat, San Jose CA).

Patch-clamp recording in brain slices

WT and homozygous α4L9′A mice were anesthetized with CO_2 and decapitated. Brains were removed and a block of tissue containing the habenula was placed in ice-cold artificial cerebrospinal fluid (ACSF) containing in mM: NaCl, 126; $NaHCO_3$, 26; KCl, 2.5;

NaH_2PO_4, 1.25; $MgCl_2$, 1; $CaCl_2$, 2; D-glucose, 25; kynurenic acid, 1; bubbled with 95% CO_2 / 5% O_2. The tissue was glued to the slicing platform of a DSK-1000 vibratome tissue slicer (Dosaka EM, Kyoto, Japan), and immersed in ACSF. Four to six coronal slices containing the MHb were maintained for 1 - 8 h in the pre-chamber, then individually transferred to a recording chamber mounted to the fixed stage of an Olympus microscope equipped with DIC optics and an infra-red-sensitive camera and continuously perfused with ACSF at 1–2 ml min^{-1}.

MHb cell recordings were obtained from either the ventromedial area close to the 3rd ventricle or the ventrolateral area adjacent to the lateral habenula (see fluorescence in figure 1). Patch pipettes contained in mM: K- or Cs-gluconate, 144; HEPES, 10; EGTA, 0.2; $MgCl_2$, 3; pH 7.2. Series resistance (uncompensated) and whole-cell capacitance were monitored throughout the recording. Voltage-clamp currents were recorded using an AxoPatch (Molecular Devices Axon Instruments) amplifier, filtered at 1 kHz, digitized at 2 kHz and stored to disk using pCLAMP (Axon) for off-line analysis. Neurons were included in the analysis if there was < 100 pA leak at −50 mV. Nicotine (diluted in ACSF) was applied by pressure ejection (1 - 3 psi, 10 s) using a micropipette positioned < 20 μm from the cell. In some experiments, blockers were added to the ACSF to suppress other responses: tetrodotoxin (200 nM); D-AP5 (10-20 μM); CNQX (10 μM).

Results

Distribution of α4 mRNA and expression of α4-YFP receptors

The distribution of α4 mRNA and α4 protein was assessed by *in situ* hybridization in C57BL/6J mice and by fluorescence of tissue from α4YFP mice, respectively. The signal from hybridized α4 mRNA was concentrated in the ventrolateral region of the MHb, whereas no signal was detected in the dorsal-medial aspect of the structure (Figure 1 A, B). A similar distribution pattern of α4 mRNA within the MHb of C57BL/6J mice appears in the data of Wada et al (1989) and of the Allen Brain Atlas (www.brain-map.org).

The brains of α4YFP mice displayed YFP signal in several areas (Nashmi et al, 2007). The highest intensity was found in the MHb. YFP fluorescence was localized to the ventrolateral portion of the MHb, with a distribution pattern strongly resembling that of the *in situ* hybridization study (Figure 1 C, E). α4* nAChRs were also visualized in projection fibers of the fasciculus retroflexus (fr; Figure 1C, D); other images show that the YFP-fluorescence persists as these fibers reach the interpeduncular nucleus. As negative control, tissue from WT littermates of α4YFP mice showed no YFP fluorescence (data not shown).

The α4YFP mice were developed, and have been previously exploited, to provide quantitative data about protein levels. Thus, when α4YFP expression in various brain areas (Nashmi et al 2007) is compared with the known expression of L-[^{3}H]nicotine binding in those same brain regions (Marks et al 1992), α4YFP expression correlates significantly with nicotine binding ($r = 0.80$; $p = 0.0005$; Fig. 2A), as expected if α4 subunits are a major component of high affinity nicotine binding sites (Marks et al., 1992). Furthermore, in detailed previous studies of midbrain GABAergic neurons, chronic nicotine produced 30-50% increases in α4YFP fluorescence, and this corresponded well with electrophysiologically measured increases in nAChR responses (Nashmi et al, 2007). Indeed, Nashmi et al (2007) pointed out that there is a correlation coefficient, across nine brain areas, of 0.91 between the percentage upregulation of fluorescence and the percentage upregulation of nicotine binding (Marks et al, 1992; Nashmi et al, 2007). As observed here for α4 nAChR subunits, there is often a nonlinear or non-monotonic relation between mRNA expression and protein expression (Fig. 2B). Overall, the high levels of both α4 mRNA and α4YFP fluorescence suggest that, in the MHb, α4 protein

distribution closely parallels the expression of α4 subunit mRNA, and also suggest that the α4 subunit may be functionally incorporated into nAChRs within distinct regions of the MHb.

If α4 subunits normally contribute to receptors in the ventrolateral MHb then one expects cells in this region to produce especially sensitive nicotine responses in mice carrying the α4L9′A allele (Tapper et al., 2004). This hypothesis was tested by assaying low dose nicotine-induced c-fos expression *in vivo* and low concentration nicotine-evoked currents in slices.

C-fos activation in the MHb of α4L9′A mice

We assessed c-fos expression in brain sections of WT and α4L9′A mice by immunohistochemical detection. Consistent with its role as a transcription factor, c-fos expression was revealed by the accumulation of chromophore inside cell nuclei. At a dose of 0.1 mg/kg nicotine, the most conspicuous c-fos signal in the brains of α4L9′A mice was found in the MHb. Within the MHb, the ventrolateral portion displayed a high density of c-fos positive cells (119 ± 23 cells/MHb-section), while the more dorsomedial aspects were almost devoid of labeled cells (Figure 3). The MHb of WT mice injected with 0.1 mg/kg nicotine showed very few c-fos positive cells (4.4 ± 2.8 cells/MHb-section). Similar to WT injected with 0.1 mg/kg nicotine, low numbers of c-fos positive cells were found in the MHb of both WT and α4L9′A mice injected with saline solution (WT: 7.0 ± 1.4, α4L9′A: 4.3 ± 1.1 cells/MHb-section). A dose of 0.1 mg/kg nicotine elicited no observable behavioral effects in WT, while some (2 out of 5) α4L9′A mice injected with the same dose displayed Straub tail (curving of the tail over the back).

In α4L9′A mice, nicotine injections at doses higher than > 0.1 mg/kg revealed heavier and more widespread c-fos labeling in the MHb (Fig. 4) as well as in other brain regions. Thus, at 10 mg/kg, all regions of the MHb from WT mice showed c-fos labeling (Fig. 4C). At the intermediate dose of 2 mg/kg, dorsomedial cells of the MHb were still much more heavily labeled in MHb of L9′A than of WT mice (Figure 4A, B). These data imply that, in WT mice, despite possible differences in subunit composition, nAChRs in all parts of the ventral MHb are equally sensitive to threshold concentrations of nicotine (see also electrophysiological evidence in Fig. 5; Quick et al., 1999). However, interpretation of data at these higher doses of nicotine is likely complicated by previously reported motor responses such as stereotypy and tremors (Fonck et al, 2005). Correlations between c-fos expression in the brains of α4L9′A mice and the resulting behavioral responses (for example, seizures at 1 mg/kg nicotine) will be the subject of a separate study. Young (P14 to P20, similar to animals used for electrophysiology) α4L9′A (n = 3) and WT mice (n = 2) were analyzed for c-fos expression in the MHb following a 0.1 mg/kg nicotine injection, revealing a similar expression pattern to that of adult mice (data not shown).

Patch-clamp recording in the MHb of α4L9′A mice

In neurons from the MHb of WT mice, a low concentration of nicotine (1 μM) evoked small inward or no currents at holding potentials of -50 to -90 mV, irrespective of the location of the cell. Figures 5A, B show exemplar traces; and Figure 5C shows all data. These findings indicate that all neurons in the WT ventral MHb have roughly equal sensitivity to a low concentration (1 μM) of agonist (see Quick et al., 1999), but provide no information on differential subunit composition of nAChRs. If, however, α4 subunits participate in a functional receptor population, we would expect larger responses in α4L9′A mice. This result was indeed realized. In slices obtained from the α4L9′A animals, all ventrolateral MHb cells showed greatly enhanced responses to 1 μM nicotine (Figure 5A, right trace; Figure 5C); but ventromedial MHb cells (Figure 5B, right trace), displayed currents not significantly different in amplitude from ventromedial MHb cells in WT mice (Figure 5C). These data are consistent with the

inclusion of α4 subunits into functional nAChRs on cells in the ventrolateral but not the ventromedial parts of the MHb.

Discussion

These studies illustrate how genetic approaches using knock-in mice that express fluorescent or hypersensitive nicotinic receptors can help identify the functional contribution of individual subunit genes to heteromultimeric receptors in specified neurons. Our results indicate that functional nAChRs containing α4 subunits are selectively localized to cells in the ventrolateral region of the MHb. This conclusion is based on a consistent set of four observations: the patterns of α4 mRNA labeling in WT MHb; the patterns of highly sensitive nicotine-induced c-fos reactivity in MHb neurons from mice expressing hypersensitive α4L9′A subunit genes; the patterns of highly sensitive nicotine-elicited currents in MHb neurons from mice expressing hypersensitive α4L9′A subunit genes; and the distribution of YFP-tagged α4* nAChRs in α4YFP mice. Previous data on the two knock-in lines provide ample assurance that neither the hypersensitive L9′A mutation nor the introduced YFP moiety alter the expression patterns of α4* nAChRs or the incorporation of α4 subunits into nAChRs (Tapper et al., 2004; Fonck et al, 2005; Tapper et al, 2007; Nashmi et al, 2007; Shao et al., 2008). Subunit composition analysis based on gain-of-function knock-in may be extended to other nAChR subunit genes or other ligand-gated ion channels.

These gain-of-function analyses complement pharmacological studies, especially because there are few agonists, antagonists, or allosteric modulators selective for single nAChR subtypes. The MHb is among a group of brain regions that may not express the otherwise dominant α4β2* nAChR subtype(s) (Marks et al., 1998; Perry et al., 2002). Previous studies concluded that a plurality of receptors in this nucleus contain an α3β4 ligand-binding interface, based on the strong potency of cytisine (Mulle and Changeux, 1990), and the high sensitivity to the α-conotoxin AuIB (Quick et al., 1999). The present data suggest the presence of an additional component: an α4* population of nAChRs within the ventrolateral MHb. The c-fos stereology data, combined with the knowledge that the MHb is ~1.8 mm in length, allow us to estimate that this population is ~7200 neurons per mouse MHb. Which non-α subunit(s) partner with MHb α4 to form functional receptors? The α4β2 subunit combination, widely distributed in the rest of the brain, appears unlikely because β2 knockout mice retain nicotinic responses in MHb (Picciotto et al., 1995). Given the preponderance of β4 in the MHb, we speculate that α4β4* receptors predominate in the ventrolateral MHb, while the α3β4* subtype (s) is more prevalent in the medial MHb.

The α4L9′A mice are an exon replacement knock-in strain and do not overexpress receptors. As shown by Tapper et al (2004) and by Fonck et al (2005), α4L9′A are present at normal to modestly less than normal levels; non-cytisine-sensitive high-affinity receptors are also present at normal levels. The α4L9′A mice develop normally in all respects. While they are hypersensitive to exogenously administered nicotine, ACh itself is eliminated within ~1 ms by endogenous acetylcholinesterase. Consistent with these points, previous data show that the alpha4L9′A mice have only subtly changed baseline physiology, such as a dihydro-β-erythroidine-sensitive breathing frequency (Shao et al, 2008). It is therefore unlikely that functional compensation occurs in the medial habenula of the α4L9′A strain by alterations in the expression of other receptors or subunits.

Interestingly, the major projections of the ventral part of the MHb to the interpeduncular nucleus (IPN) can be divided roughly in keeping with our suggested distribution of α4* and non-α4* receptor subtypes. There is a striking retrograde labeling of the ventrolateral MHb that parallels the fluorescent staining (fr; Figure 1C) after the caudal/lateral parts of the IPN are injected with dye (Contestabile and Flumerfelt, 1981). This appears to be the dominant

MHb projection to the IPN, whereas the more medial cell populations seem to project to the central parts of the IPN (Contestabile and Flumerfelt, 1981). Thus activation of the different nAChRs regions of the MHb may be associated with differential activation of the subnuclear regions of the IPN, with a corresponding heterogeneity of physiological and behavioral effects (Morley, 1986)

Overall, the functional relevance of the MHb is not well understood, although given the cholinergic phenotype of cells in ventral portions of this nucleus, it is likely to be involved in behavioral processes, such as reward, sleep-wake cycles and learning and memory, that involve the relay of cholinergic information from the forebrain to the midbrain (Woolf & Butcher, 1985; Lecourtier and Kelly 2007). Perhaps the differential expression of nAChR subtypes within medial and lateral regions of the MHb, coupled with distinct efferent targets, allows the MHb-IPN system to organize these different behaviors. For example, it is tempting to speculate that the presence of two distinct β4-containing receptors in the medial and lateral MHb may segregate distinct aspects of addiction, e.g., sensitization, drug-seeking and modulation of withdrawal symptoms (Salas et al, 2003; Salas et al., 2004; Glick et al., 2006; Taraschenko et al., 2007).

Acknowledgements

This work was supported by PHS grants NS31669, DA17173, DA17279, California Tobacco-Related Disease Research Project, and the Philip Morris External Research Fund. R.N. was supported by a NARSAD Young Investigator Award.

References

Arneric SP, Holladay M, Williams M. Neuronal nicotinic receptors: a perspective on two decades of drug discovery research. Biochemical Pharmacology 2007;74:1092–1101. [PubMed: 17662959]

Brussaard AB, Yang X, Doyle JP, Huck S, Role LW. Developmental regulation of multiple nicotinic AChR channel subtypes in embryonic chick habenula neurons: contributions of both the α2 and α4 subunit genes. Pflugers Archives 1994;429:27–43. [PubMed: 7708479]

Connolly JG, Gibb AJ, Colquhoun D. Heterogeneity of neuronal nicotinic acetylcholine receptors in thin slices of rat medial habenula. Journal of Physiology 1995;484:87–105. [PubMed: 7541465]

Contestabile A, Flumerfelt BA. Afferent connections of the interpeduncular nucleus and the topographic organization of the habenulo-interpeduncular pathway: an HRP study in the rat. Journal of Comparative Neurology 1981;196:253–270. [PubMed: 7217357]

Cordero-Erausquin M, Marubio LM, Klink R, Changeux JP. Nicotinic receptor function: new perspectives from knockout mice. Trends in Pharmacological Sciences 2000;21:211–217. [PubMed: 10838608]

Fonck C, Cohen BN, Nashmi R, Whiteaker P, Wagenaar DA, Rodrigues-Pinguet N, Deshpande P, McKinney S, Kwoh S, Munoz J, Labarca C, Collins AC, Marks MJ, Lester HA. Novel seizure phenotype and sleep disruptions in knock-in mice with hypersensitive α4* nicotinic receptors. Journal of Neuroscience 2005;25:11396–11411. [PubMed: 16339034]

Fonck C, Nashmi R, Deshpande P, Damaj MI, Marks MJ, Riedel A, Schwarz J, Collins AC, Labarca C, Lester HA. Increased sensitivity to agonist-induced seizures, Straub tail, and hippocampal theta rhythm in knock-in mice carrying hypersensitive α4 nicotinic receptors. Journal of Neuroscience 2003;23:2582–2590. [PubMed: 12684443]

Glick SD, Ramirez RL, Livi JM, Maisonneuve IM. 18-Methoxycoronaridine acts in the medial habenula and/or interpeduncular nucleus to decrease morphine self-administration in rats. European Journal of Pharmacology 2006;537:94–98. [PubMed: 16626688]

Gotti C, Moretti M, Gaimarri A, Zanardi A, Clementi F, Zoli M. Heterogeneity and complexity of native brain nicotinic receptors. Biochemical Pharmacology 2007;74:1102–1111. [PubMed: 17597586]

Janes RW. α-Conotoxins as selective probes for nicotinic acetylcholine receptor subclasses. Current Opinions in Pharmacology 2005;5:280–292.

Lecourtier L, Kelly PH. A conductor hidden in the orchestra? Role of the habenular complex in monoamine transmission and cognition. Neuroscience and Biobehavior Reviews 2007;31:658–672.

Luetje CW. Getting past the asterisk: the subunit composition of presynaptic nicotinic receptors that modulate striatal dopamine release. Molecular Pharmacology 2004;65:1333–1335. [PubMed: 15155826]

Marks MJ, Smith KW, Collins AC. Differential agonist inhibition identifies multiple epibatidine binding sites in mouse brain. Journal of Pharmacology and Experimental Therapeutics 1998;285:377–386. [PubMed: 9536034]

Marks MJ, Pauly JR, Gross SD, Deneris ES, Hermans-Borgmeyer I, Heinemann SF, Collins AC. Nicotine binding and nicotinic receptor subunit RNA after chronic nicotine treatment. Journal of Neuroscience 1992;12:2765–2784. [PubMed: 1613557]

Maskos U, Molles BE, Pons S, Besson M, Guiard BP, Guilloux JP, Evrard A, Cazala P, Cormier A, Mameli-Engvall M, Dufour N, Cloëz-Tayarani I, Bemelmans AP, Mallet J, Gardier AM, David V, Faure P, Granon S, Changeux JP. Nicotine reinforcement and cognition restored by targeted expression of nicotinic receptors. Nature 2005;436:103–107. [PubMed: 16001069]

Morley BJ. The interpeduncular nucleus. International Review of Neurobiology 1986;28:157–182. [PubMed: 2433243]

Mulle C, Changeux JP. A novel type of nicotinic receptor in the rat central nervous system characterized by patch-clamp techniques. Journal of Neuroscience 1990;10:169–175. [PubMed: 2299390]

Nashmi R, Dickinson ME, McKinney S, Jareb M, Labarca C, Fraser SE, Lester HA. Assembly of α4β2 nicotinic acetylcholine receptors assessed with functional fluorescently labeled subunits: effects of localization, trafficking, and nicotine-induced upregulation in clonal mammalian cells and in cultured midbrain neurons. Journal of Neuroscience 2003;23:11554–11567. [PubMed: 14684858]

Nashmi R, Xiao C, Deshpande P, McKinney S, Grady SR, Whiteaker P, Huang Q, McClure-Begley T, Lindstrom JM, Labarca C, Collins AC, Marks MJ, Lester HA. Chronic nicotine cell specifically upregulates functional α4* nicotinic receptors: basis for both tolerance in midbrain and enhanced long-term potentiation in perforant path. Journal of Neuroscience 2007;27:8202–8218. [PubMed: 17670967]

Pauly JR, Marks MJ, Robinson SF, Van de Kamp JL, Collins AC. Chronic nicotine and mecamylamine treatment increase brain nicotinic receptor binding without changing α4 or β2 mRNA levels. Journal of Pharmacology and Experimental Therapeutics 1996;278:361–369. [PubMed: 8764371]

Perry DC, Xiao Y, Nguyen HN, Musachio JL, Dávila-García MI, Kellar KJ. Measuring nicotinic receptors with characteristics of α4β2, α3β2 and α3β4 subtypes in rat tissues by autoradiography. Journal of Neurochemistry 2002;82:468–481. [PubMed: 12153472]

Phillips HA, Scheffer IE, Berkovic SF, Hollway GE, Sutherlan GR, Mulley JC. Localization of a gene for autosomal dominant nocturnal frontal lobe epilepsy to chromosome 20q13.2. Nature Genetics 1995;10:117–118. [PubMed: 7647781]

Picciotto MR, Zoli M, Léna C, Bessis A, Lallemand Y, Le Novère N, Vincent P, Pich EM, Brûlet P, Changeux JP. Abnormal avoidance learning in mice lacking functional high-affinity nicotine receptor in the brain. Nature 1995;374:65–67. [PubMed: 7870173]

Picciotto MR, Caldarone BJ, Brunzell DH, Zachariou V, Stevens TR, King SL. Neuronal nicotinic acetylcholine receptor subunit knockout mice: physiological and behavioral phenotypes and possible clinical implications. Pharmacology and Therapeutics 2001;92:89–108. [PubMed: 11916531]

Quick MW, Ceballos MR, Kasten M, McIntosh MJ, Lester RAJ. α3β4 subunit-containing nicotinic receptors dominate function in rat medial habenula neurons. Neuropharmacology 1999;38:769–783. [PubMed: 10465681]

Role LW. Diversity in primary structure and function of neuronal nicotinic acetylcholine receptor channels. Current Opinions Neurobiology 1992;2:254–262.

Salas R, Pieri F, Fung B, Dani JA, De Biasi M. Altered anxiety-related responses in mutant mice lacking the β4 subunit of the nicotinic receptor. Journal of Neuroscience 2003;23:6255–6263. [PubMed: 12867510]

Salas R, Pieri F, De Biasi M. Decreased signs of nicotine withdrawal in mice null for the β4 nicotinic acetylcholine receptor subunit. Journal of Neuroscience 2004;24:10035–10039. [PubMed: 15537871]

Shao XM, Tan W, Xiu J, Puskar N, Fonck C, Lester HA, Feldman JL. α4* Nicotinic receptors in preBötzinger complex mediate cholinergic/nicotinic modulation of respiratory rhythm. Journal of Neuroscience 2008;28:519–528. [PubMed: 18184794]

Sheffield EB, Quick MW, Lester RAJ. Nicotinic acetylcholine receptor subunit mRNA expression and channel function in medial habenula neurons. Neuropharmacology 2000;39:2591–2603. [PubMed: 11044729]

Tapper AR, McKinney SL, Nashmi R, Schwarz J, Deshpande P, Labarca C, Whiteaker P, Marks MJ, Collins AC, Lester HA. Nicotine activation of α4* receptors: sufficient for reward, tolerance, and sensitization. Science 2004;306:1029–1032. [PubMed: 15528443]

Tapper A, McKinney S, Marks M, Lester H. Nicotine responses in hypersensitive and knockout α4 mice account for tolerance to both hypothermia and locomotor suppression in wild-type mice. Physiological Genomics 2007;3:422–428. [PubMed: 17712039]

Taraschenko OD, Shulan JM, Maisonneuve IM, Glick SD. 18-MC acts in the medial habenula and interpeduncular nucleus to attenuate dopamine sensitization to morphine in the nucleus accumbens. Synapse 2007;61:547–560. [PubMed: 17447255]

Wada E, Wada K, Boulter J, Deneris E, Heinemann S, Patrick J, Swanson LW. Distribution of α2, α3, α4, and β2 neuronal nicotinic receptor subunit mRNAs in the central nervous system: a hybridization histochemical study in the rat. Journal of Comparative Neurology 1989;284:314–335. [PubMed: 2754038]

Whiteaker P, Peterson CG, Xu W, McIntosh JM, Paylor R, Beaudet AL, Collins AC, Marks MJ. Involvement of the α3 subunit in central nicotinic binding populations. Journal of Neuroscience 2002;22:2522–2529. [PubMed: 11923417]

Woolf NJ, Butcher LL. Cholinergic systems in the rat brain: II. Projections to the interpeduncular nucleus. Brain Research Bulletin 1985;14:63–83. [PubMed: 2580607]

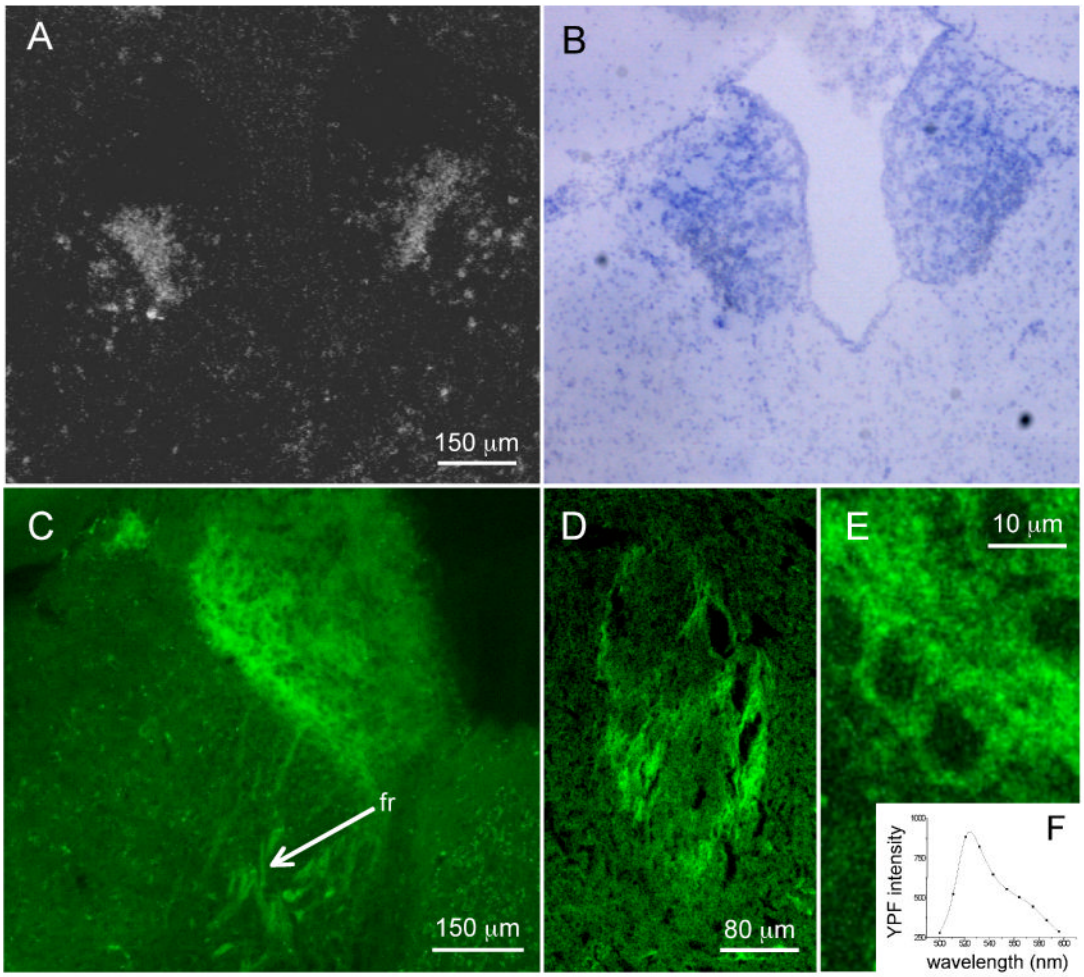

Figure 1.

In situ hybridization of α4 subunit mRNA and α4YFP fluorescence in MHb.

A cRNA ribo-probe labeled with [^{35}S]UTP was synthesized from the mouse DNA template. (A) Approximately a third of the MHb, the ventrolateral aspect, is strongly labeled by the α4 probe. (B) Same section as in (A) stained with Nissl. (C) Confocal image of an α4YFP mouse brain section with positive YFP fluorescence in the ventrolateral portion of MHb. α4YFP is also visible in axons of the fasciculus retroflexus fiber tract (fr). (D) Positive YFP fluorescence on a cross-section of the fasciculus retroflexus fiber track (oval shaped). (E) High-power image showing α4YFP in individual MHb neurons. (F) Spectrum (wavelength versus YFP intensity) of the fluorescence from the MHb of an α4YFP mouse brain section indicating specific YFP signal.

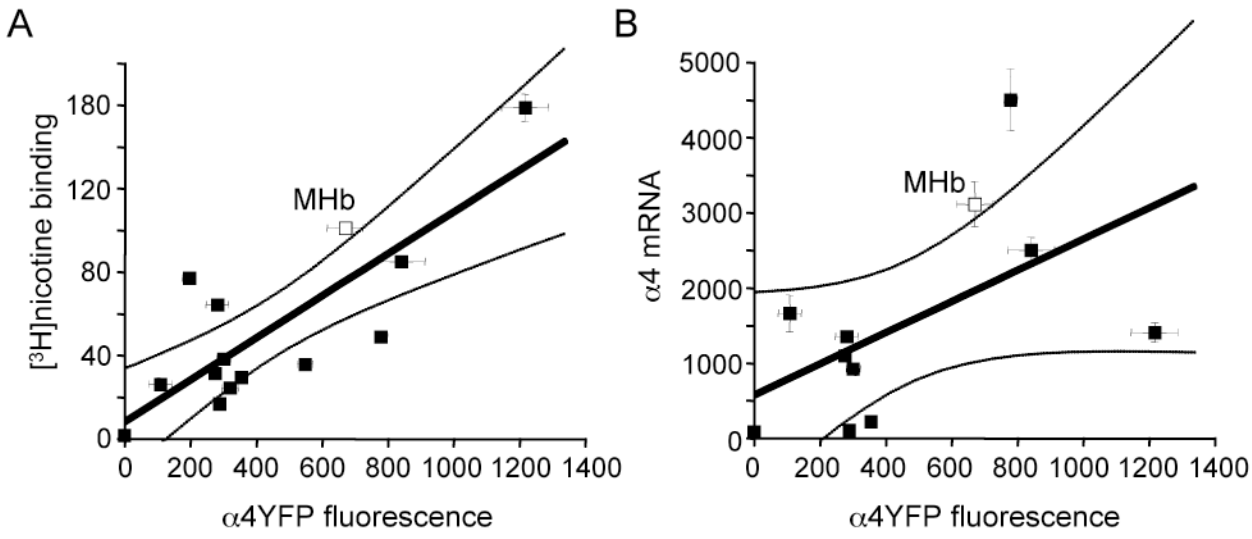

Figure 2.

Relationship between α4YFP fluorescence and nAChR mRNA and protein levels.

Plots of nicotine binding versus α4YFP fluorescence (A) and α4 nAChR mRNA versus α4YFP fluorescence (B) for various brain regions including a linear regression fit (solid line) and the 95% confidence intervals (lighter lines). Nicotine binding and α4 mRNA expression over various brain regions were taken from Marks et al (1992). α4YFP fluorescence expression measurements were taken from Nashmi et al (2007). Point representing the MHb is shown by the open symbol. Nicotine binding shows a significant positive correlation ($r = 0.80$; $p = 0.0005$) with α4YFP fluorescence. α4 mRNA did not correlate significantly ($r = 0.55$; $p = 0.08$) with α4YFP fluorescence.

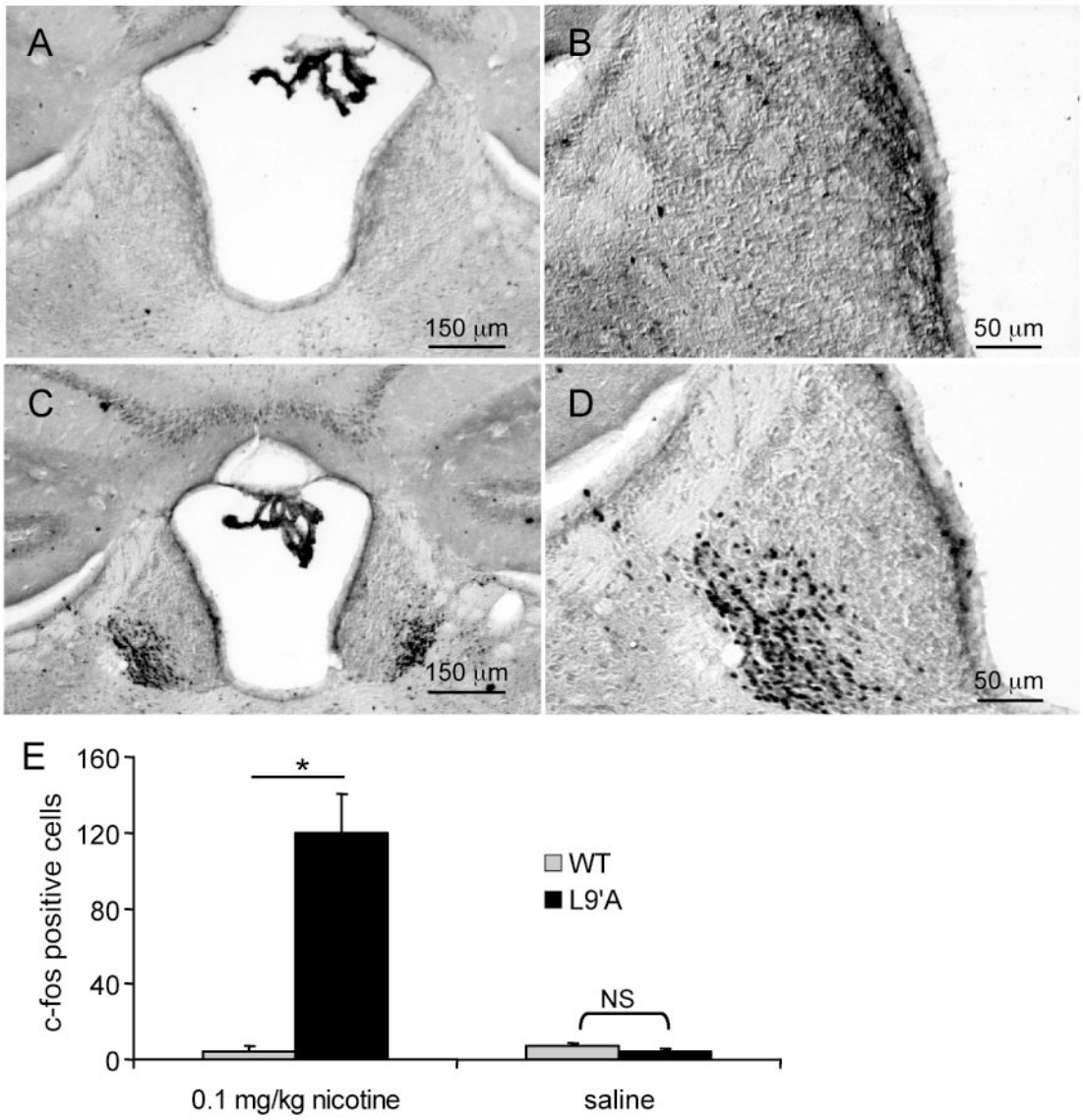

Figure 3.

C-fos immunoreactivity in WT and α4L9′A mice.

(A) Bright-field image of a coronal section of a WT mouse injected with 0.1 mg/kg nicotine showing very few c-fos labeled cells in the MHb. (B) The same section as (A) but at higher magnification. (C) C-fos immunoreactivity in MHb of an α4L9′A mouse injected with 0.1 mg/kg nicotine. Several c-fos-positive neurons are concentrated in the ventrolateral aspect of the MHb. (D) The same section as (C), but at higher magnification. (E) The average number of c-fos-positive cells within the MHb (per brain section) of mice treated with either 0.1 mg/kg nicotine or saline. There is a significant difference in the average number of c-fos labeled cells between WT and α4L9′A following a 0.1 mg/kg nicotine injection (Tukey's test, * $P < 0.0001$). Error bars indicate the S.E.M.

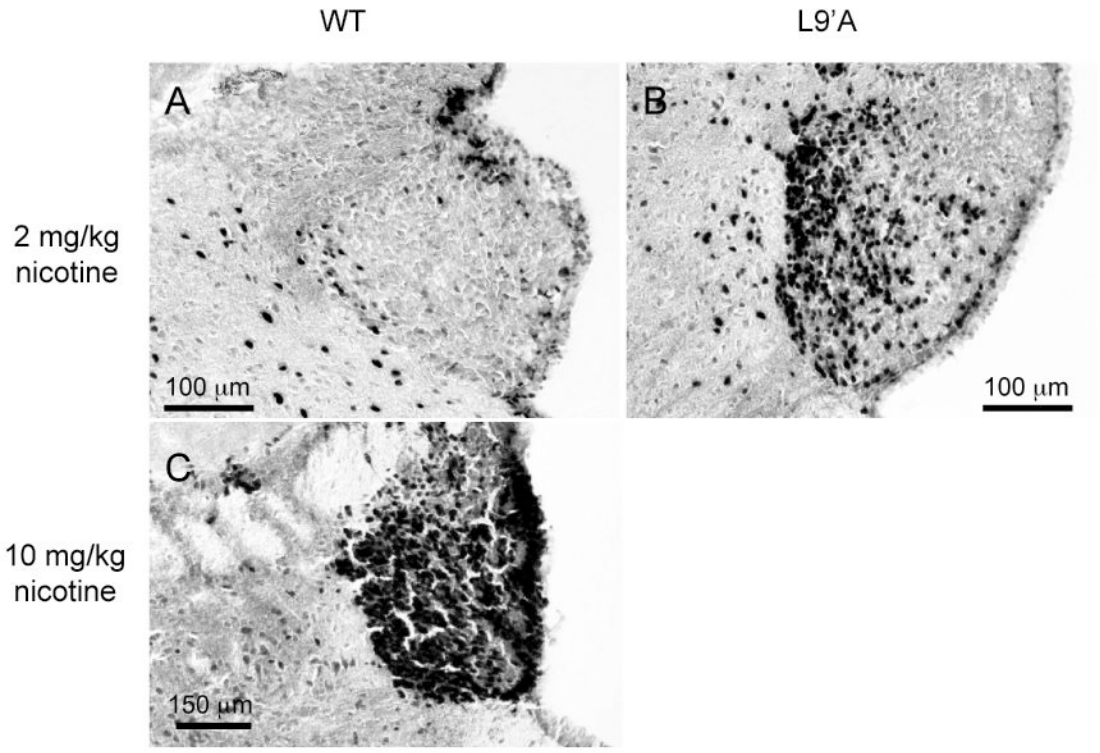

Figure 4.

C-fos immunoreactivity in WT and α4L9′A mice following treatment with high concentrations of nicotine.

Bright-field images of coronal sections of WT (A) or α4L9′A (B) mice injected with 2 mg/kg nicotine showing differences in the number of c-fos labeled cells especially in the ventrolateral aspect of the MHb. Bright-field images of coronal sections of WT (C) mice injected with 10 mg/kg nicotine showing extensive c-fos labeling throughout the ventral portion of the MHb. All animals experienced seizures at the 10 mg/kg dose of nicotine, (α4L9′A but not WT mice died following seizures and their brains were not processed further for c-fos). The α4L9′A but not WT mice exhibited seizures at 2 mg/kg (see Fonck et al., 2005).

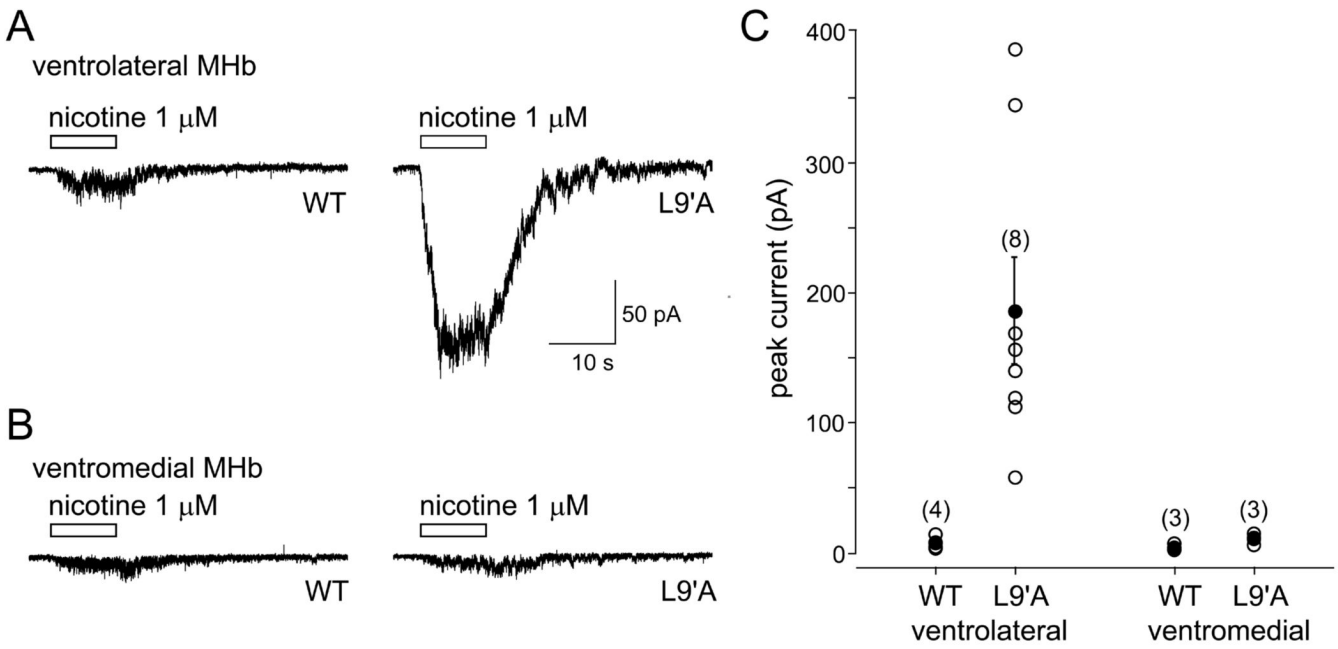

Figure 5.

Comparison of nAChR function in MHb neurons from wild-type and α4L9′A mice. Examples of currents evoked by 1 μM nicotine (10 s puffs) in lateral (A) or medial (B) MHb cells from WT (*left traces*) and α4L9′A (*right traces*) mice. Holding potential was -50 mV. (C) Scatter plot showing the distribution of current amplitudes. Open circles indicate the mean current for an individual cell. Filled circles show the group mean. Error bars indicate the S.E.M. Numbers in parentheses represent the number of cells.